Room-temperature storage of quantum entanglement using decoherence-free subspace in a solid-state spin system

F. Wang,[1] Y.-Y. Huang,[1] Z.-Y. Zhang,[1,2] C. Zu,[1] P.-Y. Hou,[1] X.-X. Yuan,[1] W.-B. Wang,[1] W.-G. Zhang,[1] L. He,[1] X.-Y. Chang,[1] and L.-M. Duan[1,2]

[1]*Center for Quantum Information, IIIS, Tsinghua University, Beijing 100084, PR China*
[2]*Department of Physics, University of Michigan, Ann Arbor, Michigan 48109, USA*
(Received 14 June 2017; revised manuscript received 20 August 2017; published 31 October 2017)

We experimentally demonstrate room-temperature storage of quantum entanglement using two nuclear spins weakly coupled to the electronic spin carried by a single nitrogen-vacancy center in diamond. We realize universal quantum gate control over the three-qubit spin system and produce entangled states in the decoherence-free subspace of the two nuclear spins. By injecting arbitrary collective noise, we demonstrate that the decoherence-free entangled state has coherence time longer than that of other entangled states by an order of magnitude in our experiment.

I. INTRODUCTION

Decoherence caused by the system-environment interaction poses a serious obstacle to physical implementation of quantum information processing [1,2]. Strategies involving active interventions, such as dynamical decoupling [3–10] and quantum error correction [11–14], have been extensively studied in experiments to recover quantum information from coupling with the environment [15–18]. Meanwhile, passive error control methods with no active recovery have also been proved to be efficient in preventing collective decoherence caused by symmetric system-environment coupling [19–26]. Quantum information in the decoherence-free subspace (DFS) does not decohere and is well protected even with perturbation in the system-environment interaction, making DFS an ideal quantum memory. DFS has been demonstrated in several experimental systems to protect single qubits from collective dephasing [27–31].

In this paper we present an experimental demonstration of DFS in a room-temperature solid-state system and use DFS to store quantum entanglement against general collective noise including both dephasing and dissipation. Quantum storage of single qubits has been demonstrated in a number of experimental systems, including trapped ions [32], single nuclear spins [31], and atomic or spin ensembles [33–35]. To realize the full capability of quantum memory, it is important to further extend the information storage from single qubits to quantum entanglement. This extension is not straightforward as the best quantum memories demonstrated so far typically require good isolation of the qubits, which makes it difficult to generate entanglement between the qubits in the same system. Entanglement between nuclear spins coupled to the NV centers have been created in multiple works [17,31,36–39]. Here we extend these works by demonstrating room-temperature storage of quantum entanglement in the DFS with two nuclear spins and the effectiveness of DFS under general collective noise. We produce entanglement between the nuclear spins within the DFS through universal gate control on the electronic and the nuclear spins. Under general collective noise, we demonstrate that the entangled state in DFS has coherence time longer than that of other entangled states by an order of magnitude.

II. RESULTS

A. Decoherence-free subspace

A DFS takes advantage of qubit-permutation symmetry in the system-environment interaction to isolate the stored quantum information from the environment. Therefore, evolution of quantum states inside a DFS is purely unitary. A simple example for a DFS is provided by the two-qubit subspace spanned by $|0\rangle_D = |0\rangle_{n1}|1\rangle_{n2}$ and $|1\rangle_D = |1\rangle_{n1}|0\rangle_{n2}$ when these two qubits are subject to collective dephasing noise [19,20]. Apparently, a collective random phase ϕ accumulated for the basis states $|0\rangle \rightarrow e^{i\phi}|0\rangle, |1\rangle \rightarrow e^{-i\phi}|1\rangle$ cancel out in this subspace. Most of the experimental demonstrations focus on this special case [27,28]. Under general collective noise including both dephasing and relaxation, the states $|0\rangle_D$ and $|1\rangle_D$ are not stable any more, but their combination, the singlet state $|S\rangle = (|0\rangle_{n1}|1\rangle_{n2} - |1\rangle_{n1}|0\rangle_{n2})/\sqrt{2}$, is still an entangled state lying within the DFS [22–24].

B. Control of two weakly coupled nuclear spins

We use two C^{13} nuclear spins weakly coupled to an individual NV center electronic spin in a diamond crystal as our qubits [Figs. 1(a) and 1(b)]. The NV electronic spin is a well characterized spin 1 system which can be optically initialized and readout [40], and coherently manipulated with microwave source at room temperature [41]. We use the NV electronic spin as a handle to coherently control and entangle the nuclear spins and read out their final state [39,42,43]. The external magnetic field provides a source of collective dephasing noise to the target nuclear spins. We prepare two typical entangled states $|T\rangle = (|0\rangle_{n1}|1\rangle_{n2} + |1\rangle_{n1}|0\rangle_{n2})/\sqrt{2}$ and $|S\rangle = (|0\rangle_{n1}|1\rangle_{n2} - |1\rangle_{n1}|0\rangle_{n2})/\sqrt{2}$ to demonstrate the DFS under the collective dephasing noise and find that the memory time is limited by the electronic spin relaxation time T_1. To verify the DFS under arbitrary collective noise including both dephasing and relaxation, we realize a general collective noise model by injecting a noisy radio frequency field into the system [39,44]. Under general collective noise, we show that the entangled state $|S\rangle$ within the DFS is still well protected until the electronic spin relaxation breaks the system-environment symmetry while the state $|T\rangle$ quickly decoheres.
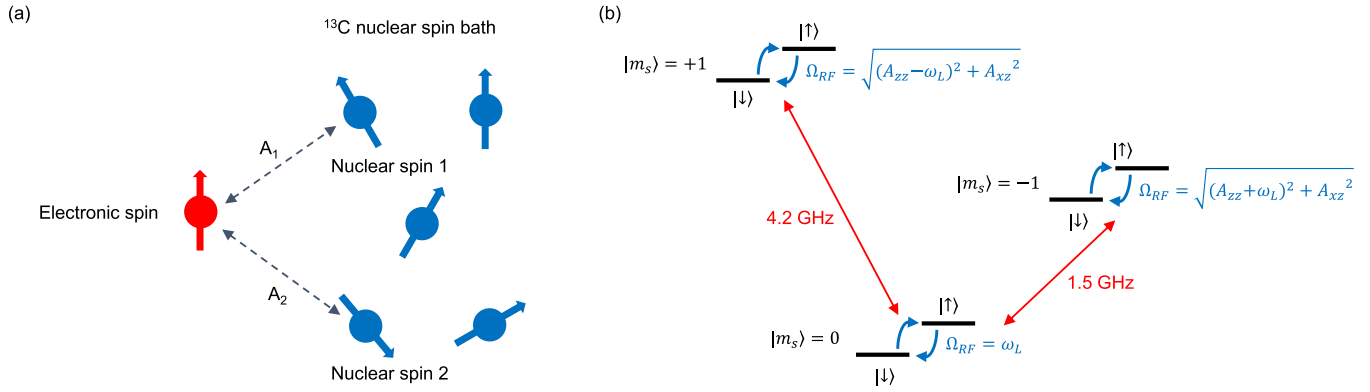
FIG. 1. Experimental system. (a) The NV electronic spin (red) and the coupled ^{13}C spin bath (blue). Entanglement states are stored in two isolated weakly coupled ^{13}C nuclear spins. (b) Energy structure of the NV electronic spin and a weakly coupled nuclear spin. Nuclear spin sublevels $|\uparrow\rangle$ and $|\downarrow\rangle$ are split by Zeeman shift (ω_L) and hyperfine interaction (A_{zz}, A_{xz}) with $\omega_0 = \omega_L(m_s = 0)$, $\omega_{\pm 1} = \sqrt{(A_{zz} \mp \omega_L)^2 + A_{xz}^2}(m_s = \pm 1)$.

The experiments are performed at room temperature on a diamond sample with an external magnetic field of 480 G along the NV symmetry axis. We use the hyperfine interaction to coherently manipulate the nuclear spin by applying an equally spaced sequence of π rotations (the Carr-Purcell-Meiboom-Gill, or CPMG sequence) to flip the electronic spin [17,18,43]. We use the $XY8$ sequence in our experiment to

reduce the influence of imperfection in pulse durations and the accumulation of systematic pulse errors [16,44]. The multipulse CPMG sequence decouples the electronic spin from the spin bath. At the same time, the electronic spin gets entangled with a specific nuclear spin when the pulse interval 2τ satisfies certain resonance condition, which leads to collapse of the electronic spin coherence after the CPMG
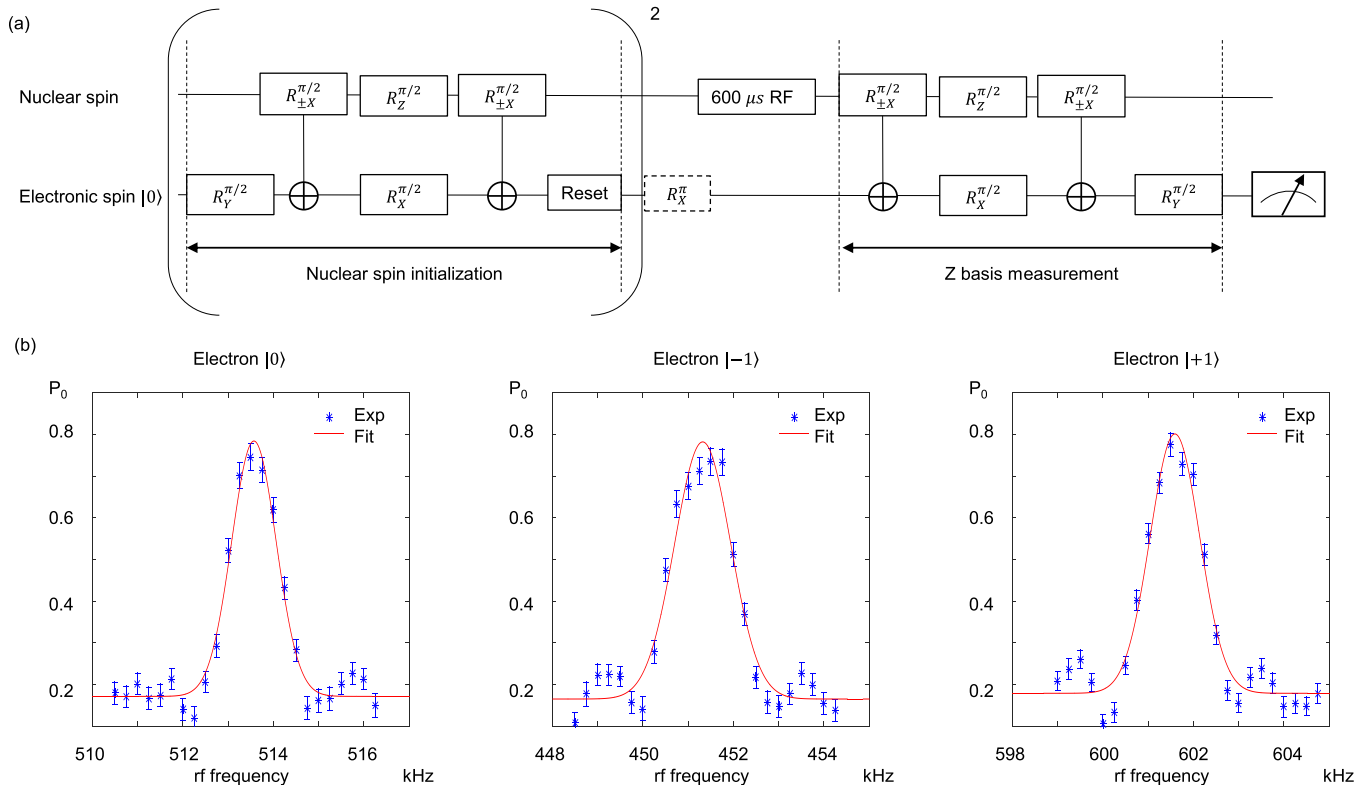

FIG. 2. Calibration of the nuclear spin hyperfine interaction parameters. (a) Gate sequence to scan the resonant frequency of nuclear spins with the electronic spin set at $m_s = +1, 0, -1$ states, respectively. The nuclear spin is initialized by swapping the electronic spin polarization onto the nuclear spin. Electronic spin is reset to $|0\rangle$ or $|\pm 1\rangle$ state using a 350 ns green laser or an additional π rotation afterwards. A rf pulse with a duration of 600 μs and a scanning frequency is then implemented on the nuclear spin to trigger spin flips at resonant frequency. The final state readout is accomplished by swapping the nuclear spin state back onto the electronic spin. (b) Probability of electronic spin in $m_s = 0$ state (P_0) as a function of the rf frequency with the electronic spin at $m_s = 0, -1, +1$ states, respectively, for nuclear spin 1. Solid lines are the Gaussian fits. See the Supplemental Material for results on the nuclear spin 2 [45].
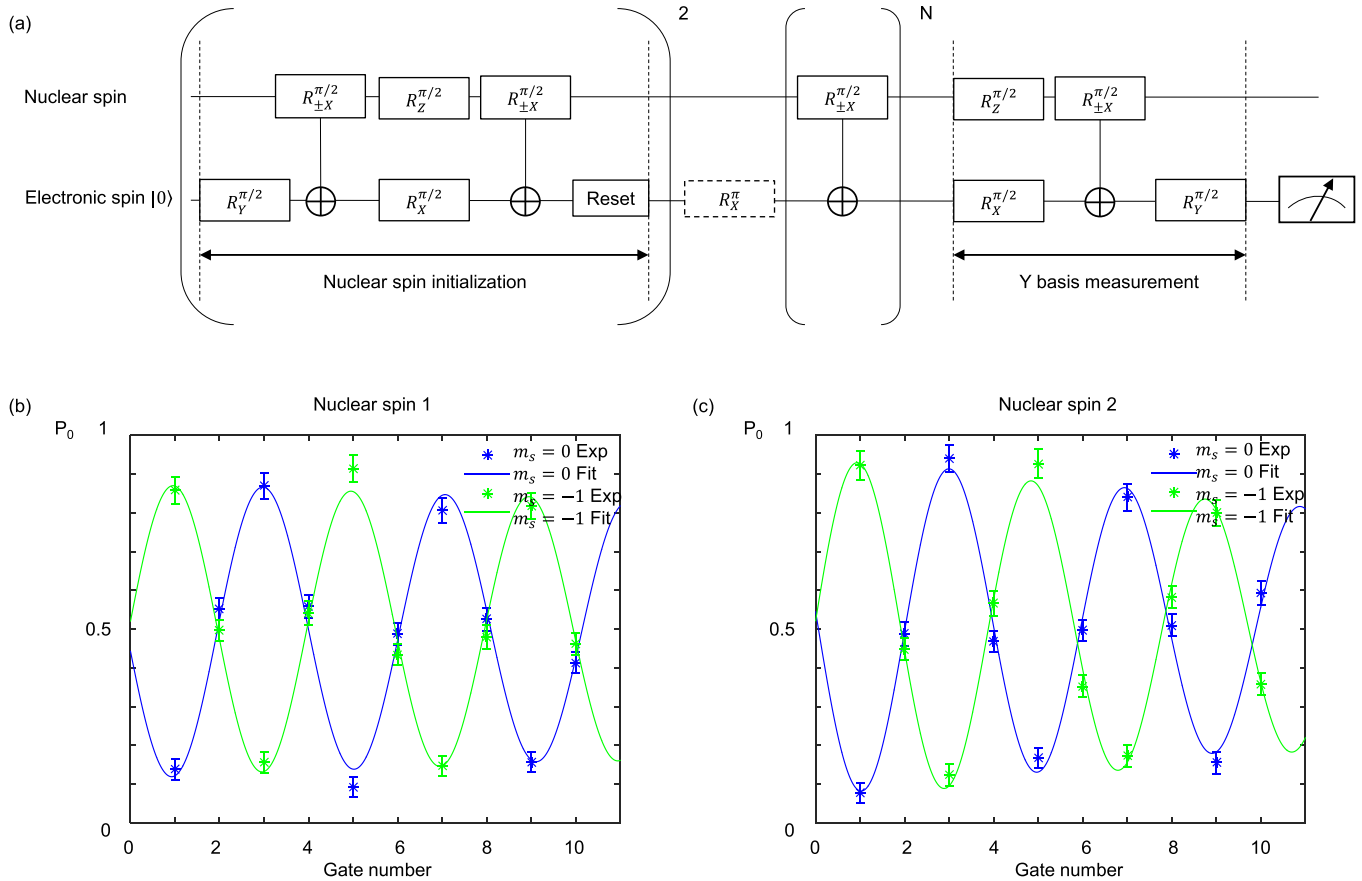
FIG. 3. Characterization of the conditional X gate on nuclear spins 1 and 2. See the Supplemental Material for results on unconditional gates [45]. (a) Experimental scheme to characterize the gate fidelity. The nuclear spin is polarized by swapping the electronic spin polarization onto the nuclear spin. An additional π rotation is applied to set the electronic spin to $m_s = -1$ state. After that, the desired gate (conditional X gate) is applied on the nuclear spin for N times ($N = 1, \ldots, 10$) with the electronic spin at $m_s = 0$ or $m_s = -1$ before measuring the nuclear spin on the Y basis. (b) and (c) Experimental results of conditional X gate on the nuclear spin 1 and 2, respectively. The nuclear spin rotates on the opposite direction of the X axis with the electronic spin at $m_s = 0, -1$ states. Solid lines are fits by the function $\sin(2\pi N/4)(1 - bN)$ with $b = 0.012$ and a standard deviation of $\sigma = 0.011$ in (b) and $b = 0.025$ and a standard deviation of $\sigma = 0.014$ in (c). The results are without correction of initialization and detection error.

sequence and thus can be detected. The resonance condition depends on $A_\parallel$, the parallel component of the hyperfine interaction for the specific nuclear spin, and is given by

$$2\tau \approx \frac{2(2k - 1)\pi}{2\omega_L + A_\parallel},$$

where the integer k denotes the order of resonance and ω_L is the nuclear spin Larmer frequency. Based on this resonance, we control the total number of π pulses N and the pulse interval 2τ to complete single-bit operations (X or Z rotation) or conditional operation ($\pm X$ rotation conditional on the state of electronic spin) on the target nuclear spins, where X and Z denote the Pauli matrices σ_x and σ_z. For each type of gate, the condition for N depends on the transverse component of the hyperfine interaction $A_\perp$ [45].

C. Calibration of hyperfine parameters

To perform high-fidelity gate operations on the weakly coupled nuclear spins, it is required to have precise calibration of the hyperfine interaction magnitudes $A_\parallel$ and $A_\perp$ for each target nuclear spins. The hyperfine parameters can be calibrated with a resolution about 10 kHz by fitting the

experimental data on the measured electronic spin coherence after the CPMG sequence to the numerical simulation of the corresponding dynamics with the fitting parameters $A_\parallel$ and $A_\perp$. However, as the gate fidelity is strongly correlated with the precision of the hyperfine parameters, the 10 kHz resolution in calibration is not enough for achieving high-fidelity quantum gates on the nuclear spins. We describe a method based on the nuclear spin ODMR (optical detected magnetic resonance) for high-precision calibration of $A_\parallel$ and $A_\perp$ in experiments. We measure the resonant frequency of the nuclear spins with the electronic spin set at $m_s = +1, 0, -1$ respectively. As described in Fig. 2(a), with rough calibration of the hyperfine parameters by the CPMG sequence, we first polarize the nuclear spin (with significant imperfection) by swapping the electronic spin polarization onto the nuclear spin, and optically reset the electronic spin to $m_s = 0$ state (or $m_s = \pm 1$ state by another resonant microwave π rotation). After that, we apply a π pulse of 600 μs duration on the target nuclear spin using radio frequency field and measure the nuclear spin flip probability by swapping the nuclear spin polarization back onto the electronic spin. In Fig. 2(b) we show that this approach gives a resonant frequency with a standard deviation of 0.05
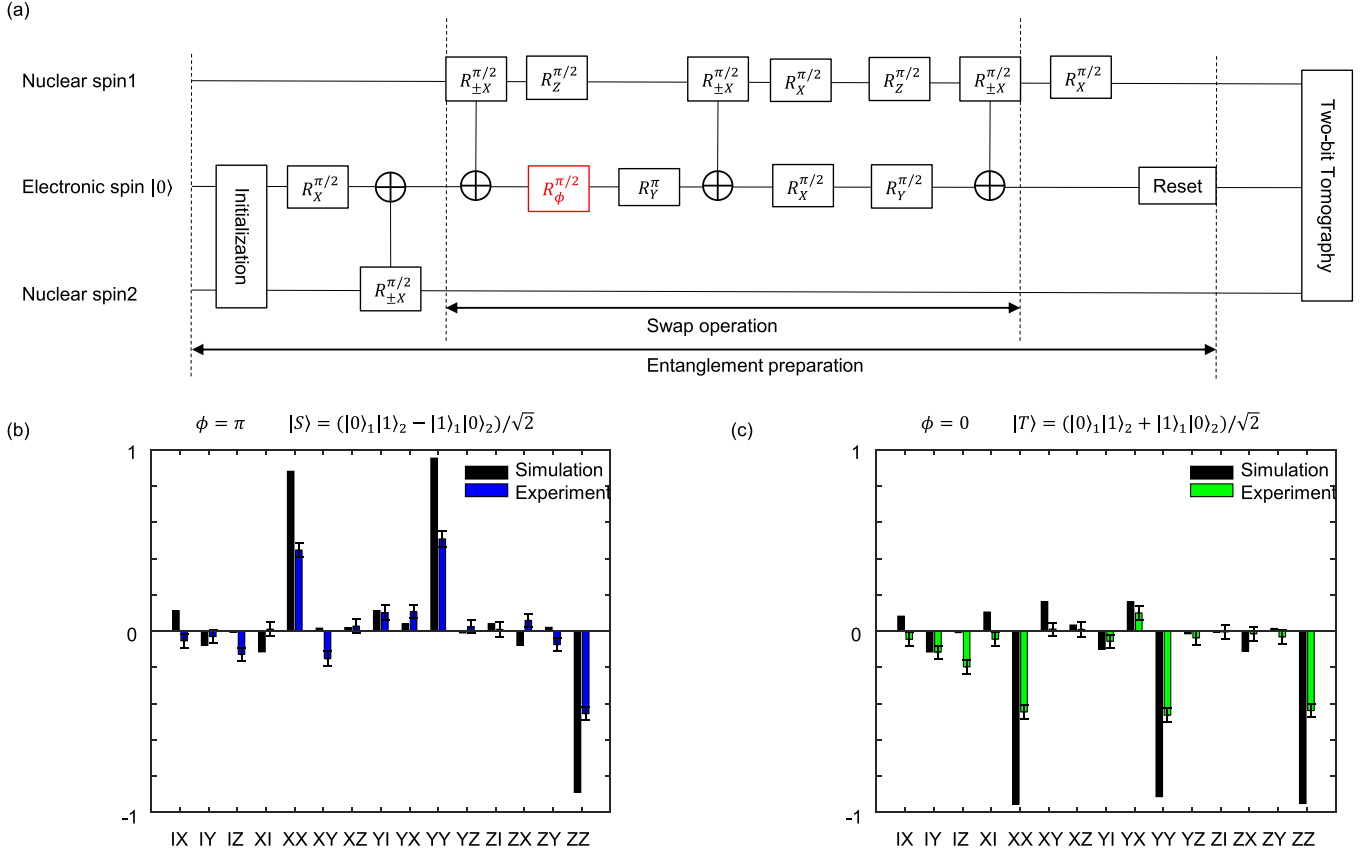
FIG. 4. Preparation and detection of entangled states between the nuclear spins. (a) Gate sequence to prepare entangled states between nuclear spins at room temperature. Entanglement is first generated between the nuclear spin 2 and the electronic spin. By swapping the electronic spin with the nuclear spin 1, entanglement between nuclear spins is produced. A subsequent $\pi/2$ rotation is applied to prepare the entangled state in the DFS. The phase ϕ of the operation in red is controlled to produce $|T\rangle$ state ($\phi = 0$) or $|S\rangle$ state ($\phi = \pi$). The readout is performed by quantum state tomography on the two nuclear spins [45]. (b) and (c) Quantum state tomography results for $|S\rangle$ state (b) and $|T\rangle$ state (c). Black bar describes the simulation result [45], blue (green) bar is the experiment data for $|S\rangle$ ($|T\rangle$) state without correction of initialization and readout errors.

kHz, which allows us to determine the nuclear spin hyperfine parameter to a resolution about 0.05 kHz in the parallel component $A_{\parallel}$ and about 0.5 kHz in the transverse component $A_{\perp}$ [45].

After the hyperfine parameters are precisely calibrated, we perform the desired gate (conditional X gate, unconditional X and Z gate) on the polarized nuclear spins with electronic spin at $m_s = 0$ or $m_s = -1$ state. To estimate the gate fidelity, we apply the same gate 10 times, and from the slow decay of the target state fidelity as shown in Fig. 3 and the Supplemental Material [45], we extract a gate fidelity about $F \approx 0.988$ ($F \approx 0.975$) for the conditional operations on nuclear spin 1 (spin 2). Gate fidelity for nuclear spin 1 is slightly higher than that for nuclear spin 2, because nuclear spin 1 has a larger parallel component of hyperfine parameters, which leads to a shorter gate time [45]. Using the high fidelity conditional X gate and the unconditional Z gate, single nuclear spin initialization and readout fidelity is enhanced to $F_1 = 0.896(6)$ and $F_2 = 0.873(9)$ for nuclear spin 1 and 2 [45].

D. Entanglement preparation

We prepare two typical entangled states $|T\rangle$ and $|S\rangle$ for the nuclear spins using the above gates. When the nuclear

spins are subject to collective dephasing noise, both states are decoherence free. However, only the entangled state $|S\rangle$ is protected under arbitrary collective noise. To produce the desired entangled states, as shown in Fig. 4(a), we first prepare an electron-nuclear entangled state $(|0\rangle_e |Y_-\rangle_{n2} - i|1\rangle_e |Y_+\rangle_{n2})/\sqrt{2}$ by applying a conditional $\pi/2$ operation on the polarized nuclear spin 2 with the electronic spin set at $(|0\rangle - i|1\rangle)/\sqrt{2}$ state, where $|Y_{\pm}\rangle$ denotes the eigenstate of σ_y with ± 1 eigenvalue. After that, we coherently swap the states between the electronic spin and the nuclear spin 1 by applying a sequence of gate operations as shown in Fig. 4(a), and subsequently implement a single-bit X gate on the nuclear spin 1 to produce the target entangled states within the DFS of the two nuclear spins. By controlling the phase ϕ of the swap gate we are able to prepare the entangled state to either $|T\rangle$ or $|S\rangle$. The entangled state fidelity is characterized by calculating the overlap between the experiment density matrix ρ_{expt} constructed through quantum state tomography [45] and the target ideal state $|\Psi_{\text{id}}\rangle$ through $F = \langle \Psi_{\text{id}} | \rho_{\text{expt}} | \Psi_{\text{id}} \rangle$. With the measured fidelity $F = 0.60(1)$ for $|S\rangle$ state and $F = 0.59(1)$ for $|T\rangle$ state (without correction of initialization and detection error), we demonstrate entanglement between the nuclear spins [Figs. 4(b) and 4(c)].
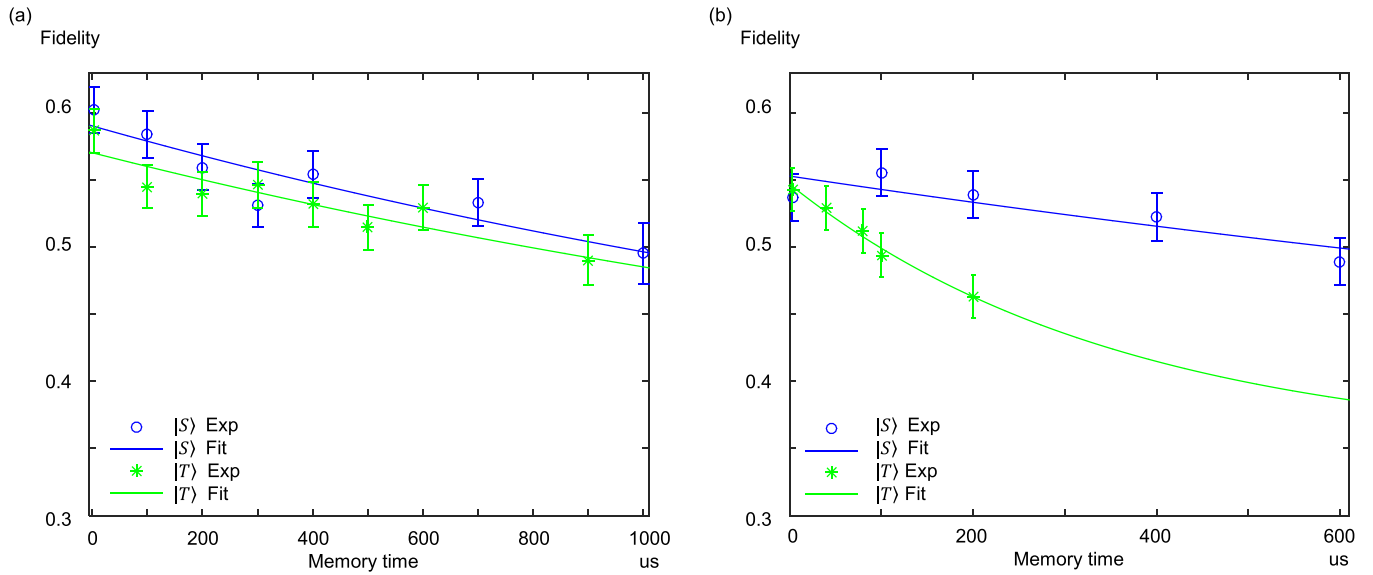
FIG. 5. Decay of the entanglement fidelity under various noise environments. (a) Entanglement fidelity as a function of the storage time t under collective dephasing noise. Solid lines are fits to $\exp(-t/T_{est})$ with $T_{est} = 2.24$ ms and a standard deviation of $\sigma = 153$ μs for $|S\rangle$ state (blue) and $T_{est} = 2.29$ ms and a standard deviation of $\sigma = 232$ μs for $|T\rangle$ state (green). The fitting curves saturate at 0.35, which corresponds to the fidelity of the final state when all the coherence terms drop to zero. Due to the limited fidelity for initial state preparation, the population is not given by an identity matrix, so the saturation fidelity is 0.35 instead of 0.5. (b) Entanglement fidelity as a function of the storage time t under general collective noise. Solid lines are fits to $\exp(-t/T_{est})$ with $T_{est} = 2.18$ ms and a standard deviation of $\sigma = 366$ μs for $|S\rangle$ state (blue) and $T_{est} = 360$ μs and a standard deviation of $\sigma = 20$ μs for $|T\rangle$ state (green).

Various imperfections affect the entangling process, which leads to a low entangled state fidelity. We summarize the four major contributions. (i) The preparation process involves the initialization of nuclear spin 2, with a single-qubit initialization and readout fidelity about 0.87, we expect a similar fidelity drop in term of the entanglement fidelity. (ii) The use of green laser at the end of the entangling process to optically reset the electronic spin decreases the nuclear spin fidelity in both polarization and coherence [17,46]. (iii) The intrinsic errors mostly caused by the crosstalk between the targeted two nuclear spins decrease the entangled state fidelity from 1 to 0.95 in our numerical simulation [see Figs. 4(b) and 4(c)]. (iv) Decoherence, magnetic field fluctuation and gate error accumulation in each experimental run (note that the whole state preparation process requires application of more than ten gates) reduce the final state fidelity over the 10^6 repetitions of experiments for measurement of each density matrix element [45]. At room temperature, due to these limitations, it is hard to significantly improve the entanglement fidelity for the nuclear spins. With an isotopically purified sample, the coherence time for the electronic spin increases, but it becomes more difficult to find nuclear spins with appropriate hyperfine interaction strength for the entangling gates. If we put the sample in a cryogenic environment, both the initialization fidelity and the coherence time for the electronic spin would be significantly improved, and correspondingly the entanglement fidelity for the nuclear spins will increase substantially [31].

E. Test of DFS under collective dephasing noise

We start by exploring DFS with the system subject to a collective dephasing noise, which in our case is the external

magnetic field. In Fig. 5(a) we prepare the nuclear spins in the DFS and measure their state fidelity extracted from quantum state tomography as a function of storage time. By fitting the data to $\exp(-t/T_{est})$, we extracted a memory time of $T_{est} \approx 2.3$ ms, which is limited by the electronic spin relaxation time $T_1 \approx 2.5$ ms. This can be explained by the breakup of the system-environment coupling symmetry. As the electronic spin relaxes, it causes independent dephasing noise for the two nuclear spins with $\Delta\omega \approx |A_{\parallel 1} - A_{\parallel 2}| \approx 148$ kHz, which destroys the state quickly [31]. Longer memory time could be achieved for entangled states if one makes use of the isotopically purified diamond samples to reduce the nuclear spin crosstalk error with spin bath and repeatedly polarizes the electronic spin to mitigate the dephasing noise [46]. Alternatively, if one put the diamond sample in the cryogenic environment, both the entanglement fidelity and entanglement storage time can be significantly improved as the electronic spin relaxation time gets much longer under low temperature [18].

F. Test of DFS under general collective noise

A crucial step to verify DFS is to investigate the state coherence under general collective noise including both dephasing and relaxation. To realize general collective noise in addition to the dephasing induced by the external magnetic field, we introduce collective relaxation by injecting a noisy radio-frequency field. Because the magnetic field couples the nuclear spins identically, the relaxation induced by the injected rf field is collective to nuclear spins in the close neighborhood of the electronic spin. In Fig. 5(b) we compare the storage time of two typical entangled states $|T\rangle$ and $|S\rangle$. In agreement with

theory, only $|S\rangle$ state which lies within the DFS under arbitrary collective noise is protected against the injected noise with a fitted memory time $T_{\text{est}} \approx 2.2$ ms. In comparison, $|T\rangle$ state is destroyed quickly with a fitted memory time $T_{\text{est}} \approx 360$ μs.

III. SUMMARY

In summary, we have demonstrated room temperature storage of quantum entanglement by preparing quantum states in the DFS of two nuclear spins and experimentally verified that the entangled state within the DFS has coherence time significantly longer than that of other components under general collective noise. Storage of quantum entanglement is required in many quantum information protocols and our result suggests that the DFS could find interesting applications in experimental realization of those protocols.

[1] W. G. Unruh, Phys. Rev. A **51**, 992 (1995).

[2] D. P. DiVincenzo, Fortschr. Phys. **48**, 771 (2000).

[3] L. Viola and S. Lloyd, Phys. Rev. A **58**, 2733 (1998).

[4] P. Zanardi, Phys. Lett. A **258**, 77 (1999).

[5] L.-M. Duan and G. Guo, Phys. Lett. A **261**, 139 (1999).

[6] D. Vitali and P. Tombesi, Phys. Rev. A **59**, 4178 (1999).

[7] L. Viola, E. Knill, and S. Lloyd, Phys. Rev. Lett. **82**, 2417 (1999).

[8] L. Viola and E. Knill, Phys. Rev. Lett. **90**, 037901 (2003).

[9] K. Khodjasteh and D. A. Lidar, Phys. Rev. Lett. **95**, 180501 (2005).

[10] H. K. Ng, D. A. Lidar, and J. Preskill, Phys. Rev. A **84**, 012305 (2011).

[11] P. W. Shor, Phys. Rev. A **52**, R2493(R) (1995).

[12] A. M. Steane, Phys. Rev. Lett. **77**, 793 (1996).

[13] A. R. Calderbank and P. W. Shor, Phys. Rev. A **54**, 1098 (1996).

[14] A. M. Steane, Proc. R. Soc. London Sect. A **452**, 2551 (1996).

[15] G. de Lange, Z. H. Wang, D. Ristè, V. V. Dobrovitski, and R. Hanson, Science **330**, 60 (2010).

[16] C. A. Ryan, J. S. Hodges, and D. G. Cory, Phys. Rev. Lett. **105**, 200402 (2010).

[17] T. H. Taminiau, J. Cramer, T. van der Sar, V. V. Dobrovitski, and R. Hanson, Nat. Nanotechnol. **9**, 171 (2014).

[18] J. Cramer, N. Kalb, M. A. Rol, B. Hensen, M. S. Blok, M. Markham, D. J. Twitchen, R. Hanson, and T. H. Taminiau, Nat. Commun. **7**, 11526 (2016).

[19] G. M. Palma, K.-A. Suominen, and A. K. Ekert, Proc. R. Soc. London Sect. A **452**, 567 (1996).

[20] L.-M. Duan and G.-C. Guo, Phys. Rev. Lett. **79**, 1953 (1997).

[21] L.-M. Duan and G.-C. Guo, Phys. Rev. A **57**, 737 (1998).

[22] P. Zanardi and M. Rasetti, Phys. Rev. Lett. **79**, 3306 (1997).

[23] P. Zanardi and M. Rasetti, Mod. Phys. Lett. B **11**, 1085 (1997).

[24] D. A. Lidar, I. L. Chuang, and K. B. Whaley, Phys. Rev. Lett. **81**, 2594 (1998).

[25] D. A. Lidar, D. Bacon, J. Kempe, and K. B. Whaley, Phys. Rev. A **63**, 022306 (2001).

[26] D. A. Lidar and K. B. Whaley, *Decoherence-Free Subspaces and Subsystems*, Springer Lecture Notes in Physics Vol. 622 (Springer, New York, 2003).

[27] P. G. Kwiat, A. J. Berglund, J. B. Altepeter, and A. G. White, Science **290**, 498 (2000).

[28] D. Kielpinski, V. Meyer, M. A. Rowe, C. A. Sackett, W. M. Itano, C. Monroe, and D. J. Wineland, Science **291**, 1013 (2001).

[29] E. M. Fortunato, L. Viola, J. Hodges, G. Teklemariam, and D. G. Cory, New J. Phys. **4**, 5 (2002).

[30] L. Viola, E. M. Fortunato, M. A. Pravia, E. Knill, R. Laflamme, and D. G. Cory, Science **293**, 2059 (2001).

[31] A. Reiserer, N. Kalb, M. S. Blok, K. J. M. van Bemmelen, T. H. Taminiau, R. Hanson, D. J. Twitchen, and M. Markham, Phys. Rev. X **6**, 021040 (2016).

[32] Y. Wang, M. Um, J.-H. Zhang, S.-M. An, M. Lyu, J.-N. Zhang, L.-M. Duan, D. Yum, and K. Kim, arXiv:1701.04195.

[33] A. I. Lvovsky, B. C. Sanders, and W. Tittel, Nat. Photon. **3**, 706 (2009).

[34] M. Zhong, M. P. Hedges, R. L. Ahlefeldt, J. G. Bartholomew, S. E. Beavan, S. M. Wittig, J. J. Longdell, and M. J. Sellars, Nature (London) **517**, 177 (2015).

[35] Y. O. Dudin, L. Li, and A. Kuzmich, Phys. Rev. A **87**, 031801(R) (2013).

[36] P. Neumann, N. Mizuochi, F. Rempp, P. Hemmer, H. Watanabe, S. Yamasaki, V. Jacques, T. Gaebel, F. Jelezko, and J. Wrachtrup, Science **320**, 1326 (2008).

[37] G. Waldherr, Y. Wang, S. Zaiser, M. Jamali, T. Schulte-Herbrüggen, H. Abe, T. Ohshima, J. Isoya, J. F. Du, P. Neumann, and J. Wrachtrup, Nature (London) **506**, 204 (2014).

[38] W. Pfaff, T. H. Taminiau, L. Robledo, H. Bernien, M. Markham, D. J. Twitchen, and R. Hanson, Nat. Phys. **9**, 29 (2013).

[39] T. van der Sar, Z. H. Wang, M. S. Blok, H. Bernien, T. H. Taminiau, D. M. Toyli, D. A. Lidar, D. D. Awschalom, R. Hanson, and V. V. Dobrovitski, Nature (London) **484**, 82 (2012).

[40] J. Wrachtrup and F. Jelezko, J. Phys.: Condens. Matter **16**, R1089 (2004).

[41] F. Jelezko, T. Gaebel, I. Popa, A. Gruber, and J. Wrachtrup, Phys. Rev. Lett. **92**, 076401 (2004).

[42] M. V. G. Dutt, L. Childress, L. Jiang, E. Togan, J. Maze, F. Jelezko, A. S. Zibrov, P. R. Hemmer, and M. D. Lukin, Science **316**, 1312 (2007).

[43] T. H. Taminiau, J. J. T. Wagenaar, T. van der Sar, F. Jelezko, V. V. Dobrovitski, and R. Hanson, Phys. Rev. Lett. **109**, 137602 (2012).

[44] F. Wang, C. Zu, L. He, W.-B. Wang, W.-G. Zhang, and L.-M. Duan, Phys. Rev. B **94**, 064304 (2016).

[45] See Supplemental Material at http://link.aps.org/supplemental/10.1103/PhysRevB.96.134314 for experimental details and numerical simulation method.

[46] L. Jiang, J. S. Hodges, J. R. Maze, P. Maurer, J. M. Taylor, D. G. Cory, P. R. Hemmer, R. L. Walsworth, A. Yacoby, A. S. Zibrov, and M. D. Lukin, Science **326**, 267 (2009).